



Edge Effects in Hypar Nets

Ivan Giorgio, Francesco Dell'Isola, David Steigmann

► To cite this version:

Ivan Giorgio, Francesco Dell'Isola, David Steigmann. Edge Effects in Hypar Nets. 2019. hal-01983998

HAL Id: hal-01983998

<https://hal.science/hal-01983998>

Preprint submitted on 16 Jan 2019

HAL is a multi-disciplinary open access archive for the deposit and dissemination of scientific research documents, whether they are published or not. The documents may come from teaching and research institutions in France or abroad, or from public or private research centers.

L'archive ouverte pluridisciplinaire **HAL**, est destinée au dépôt et à la diffusion de documents scientifiques de niveau recherche, publiés ou non, émanant des établissements d'enseignement et de recherche français ou étrangers, des laboratoires publics ou privés.

Edge Effects in Hypar Nets

Ivan Giorgio^{a,c}, Francesco dell'Isola^{a,c}, David J. Steigmann^{b,c},

^a*Dipartimento di Ingegneria Strutturale e Geotecnica, Università degli studi di Roma La Sapienza, 00184 Roma, Italy*

^b*Department of Mechanical Engineering, University of California - Berkeley, CA. 94720 USA*

^c*International Research Center for the Mathematics and Mechanics of Complex Systems, Università dell'Aquila, Italy*

Received *****, accepted after revision +++++

Presented by xxxxx

Abstract

Edge effects in hyperbolic paraboloidal nets are analyzed using a model that features elastic resistance of the fibers of the net to flexure and twist in addition to the extensional elasticity of the conventional membrane theory of networks.

To cite this article: A. Name1, A. Name2, C. R. Mecanique 333 (2005).

Résumé

Effets de bord dans les réseaux paraboloidaux hyperboliques. Les effets de bord dans les réseaux paraboloidaux hyperboliques sont analysés à l'aide d'un modèle présentant la résistance élastique des fibres du réseau à la flexion et à la torsion, en plus de l'élasticité en extension de la théorie conventionnelle des membranes pour les réseaux.

Pour citer cet article : A. Name1, A. Name2, C. R. Mecanique 333 (2005).

Key words: Second gradient models; Geodesic bending; Shell elasticity

Mots-clés : Milieux continus du second gradient; Flexion géodésique; Élasticité de la coque

1. Introduction

Hyperbolic paraboloidal (Hypar) shells are ubiquitous in the design of roofs and tension structures [1–3]. Presumably this is due to the fact that the hyperbolic paraboloid is an equilibrium shape for surfaces formed by elastic nets consisting of initially orthogonal flexible fibers. Thus, the Hypar net affords a

Email addresses: ivan.giorgio@uniroma1.it (Ivan Giorgio), francesco.dellisola@uniroma1.it (Francesco dell'Isola), dsteigmann@berkeley.edu (David J. Steigmann).

lightweight scaffold that can be used to support cladding materials used in the construction of shell structures.

The analysis of Hypar nets may be based on the membrane theory of networks in which the fibers of the net are idealized as being continuously distributed to form a surface [2, 4, 5]. In this theory the intrinsic flexural and torsional elasticities of the fibers are neglected. However, these typically give rise to localized edge effects adjacent to boundaries if the boundary constraints are not compatible with the data on position or traction that can be assigned in the membrane theory of networks. In the present work we model these effects using a 2nd-gradient model [6–11] of networks.

In Section 2 we outline the elementary theory of membrane networks and use it to show that the Hypar net furnishes an equilibrium surface. The Hypar net is also shown, in Section 3, to be an equilibrium surface in a refined 2nd-gradient theory [12, 13] that accounts for elastic resistance of the net to fiber flexure, twist and additional strain-gradient effects, provided that suitable corner forces are present in the case of a net with piecewise smooth boundary. This coincidence motivates a numerical study, in Section 4, of edge effects induced by perturbations of the boundary data relative to those associated with pure Hypar nets. These localized effects are simulated using a particular example of the refined model discussed in [12].

Reference may be made to [14–23] for recent efforts to establish models for higher-gradient continua on the basis of homogenization and their experimental validation (see, *e.g.*, [24, 25]). The continuum framework facilitates a coarse-grained description that effectively avoids local effects associated with the connectivity of a discrete network (see, *e.g.*, [26, 27]).

2. Elementary network theory

In practice it is often useful to base the analysis of elastic network structures on the continuum theory, according to which the network is identified with a surface composed of two families of continuously distributed fibers [2, 4, 5, 28–31]. The objective is then to determine the position field $\mathbf{r}(u_1, u_2)$ of the surface in equilibrium, where u_α are the Cartesian coordinates of a material point on an initial plane.

In the elementary theory each fiber family is regarded as being extensible and perfectly flexible. If the fibers are orthogonal prior to deformation, then the network may be regarded as an orthotropic membrane with a strain-energy function, per unit initial area, of the form $w(\epsilon_L, \epsilon_M, J)$, where

$$J = |L_\alpha M_\beta \mathbf{r}_{,\alpha} \times \mathbf{r}_{,\beta}|, \quad \epsilon_L = E_{\alpha\beta} L_\alpha L_\beta, \quad \epsilon_M = E_{\alpha\beta} M_\alpha M_\beta \quad (1)$$

are the areal dilation and the extensional fiber strains, and where

$$E_{\alpha\beta} = \frac{1}{2}(\mathbf{r}_{,\alpha} \cdot \mathbf{r}_{,\beta} - \delta_{\alpha\beta}), \quad (2)$$

in which $\delta_{\alpha\beta}$ is the Kronecker delta, is the Lagrange strain. Here, $\mathbf{r}_{,\alpha} = \partial \mathbf{r} / \partial u_\alpha$ and L_α and M_α ($\alpha = 1, 2$) are the Cartesian components of the unit tangent vectors to the orthogonal fibers on the initial plane.

The fiber lines on the initial plane are mapped by the deformation to

$$\lambda \mathbf{l} = \mathbf{r}_{,\alpha} L_\alpha \quad \text{and} \quad \mu \mathbf{m} = \mathbf{r}_{,\alpha} M_\alpha, \quad (3)$$

where λ and μ are the fiber stretches, and \mathbf{l} and \mathbf{m} are the unit tangents to the deformed fiber trajectories.

In standard network theory, it is assumed that the fiber families offer no resistance to shearing. The shearing angle γ is defined by $\sin \gamma = \mathbf{l} \cdot \mathbf{m}$. The areal dilation of the surface may be expressed in terms of it as $J = \lambda \mu |\cos \gamma|$. Accordingly, if the strain energy is insensitive to variations of the shear angle then it is insensitive to variations of J at fixed values of the fiber stretches, and hence a function of the form $w(\epsilon_L, \epsilon_M)$. In this case the energy is unaffected by a local collapse of the fibers onto a single trajectory

on which $\mathbf{l} \times \mathbf{m} = \mathbf{0}$. The network may be folded along such curves. Indeed, explicit solutions exhibiting this feature have been derived elsewhere [32]. The fiber strains and stretches are related simply by

$$\epsilon_L = \frac{1}{2}(\lambda^2 - 1) \quad \text{and} \quad \epsilon_M = \frac{1}{2}(\mu^2 - 1), \quad (4)$$

and so the strain energy is a function of λ and μ ; we write $w = \hat{w}(\lambda, \mu)$.

Networks are further distinguished by the absence of a Poisson effect. To see how this is manifested in the theory, we note that the energy required to stretch a unit square to dimensions λ, μ is $\hat{w}(\lambda, \mu)$. The energy required to stretch it to dimensions $\lambda + d\lambda, \mu + d\mu$ is $\hat{w} + d\hat{w}$, where $d\hat{w} = \hat{w}_\lambda d\lambda + \hat{w}_\mu d\mu$; here \hat{w}_λ and \hat{w}_μ are the forces required to produce the extension. The Poisson effect is associated with the dependence of each force on the stretch of the orthogonal family. For example, if the network exhibits a Poisson effect then the force \hat{w}_λ is sensitive to variations of the stretch μ of the orthogonal family, so that the cross-derivative $\hat{w}_{\lambda\mu}$ is non-zero. In networks, the force \hat{w}_λ is insensitive to variation of μ and $\hat{w}_{\lambda\mu}$ vanishes identically. The strain-energy function is then separable; *i.e.*, it is of the form

$$\hat{w}(\lambda, \mu) = f(\lambda) + g(\mu). \quad (5)$$

Equilibrium of the network, in the absence of distributed forces, is expressed by the partial differential equation [5]

$$\mathbf{T}_{\alpha,\alpha} = \mathbf{0}, \quad (6)$$

holding everywhere in the interior of the initial plane, where the comma is again used to refer to partial derivatives with respect to the u_α , and [5]

$$\mathbf{T}_\alpha = f'(\lambda)\mathbf{l}L_\alpha + g'(\mu)\mathbf{m}M_\alpha \quad (7)$$

are the stress vectors (forces per unit initial length). The edge condition

$$\mathbf{t} = \mathbf{T}_\alpha \nu_\alpha \quad (8)$$

applies on the boundary, where \mathbf{t} is the traction. Here ν_α are the components of the exterior unit normal to the edge. Typical boundary-value problems entail the specification of \mathbf{t} and \mathbf{r} on complementary parts of the boundary.

Suppose the fibers form a uniform rectangular grid aligned with the Cartesian coordinates on the initial plane. Then, $L_\alpha = \delta_{\alpha 1}$, $M_\alpha = \delta_{\alpha 2}$ and (6) reduces to

$$[f'(\lambda)\mathbf{l}]_{,1} + [g'(\mu)\mathbf{m}]_{,2} = \mathbf{0}, \quad (9)$$

where

$$\lambda = |\mathbf{r}_{,1}|, \quad \mathbf{l} = \lambda^{-1}\mathbf{r}_{,1}; \quad \mu = |\mathbf{r}_{,2}|, \quad \mathbf{m} = \mu^{-1}\mathbf{r}_{,2}. \quad (10)$$

Evidently any deformation for which $\mathbf{r}_{,1}$ is independent of u_1 and $\mathbf{r}_{,2}$ is independent of u_2 furnishes a solution. Moreover, these are universal in the sense that they are equilibrated in every network; *i.e.*, for all constitutive functions f and g . It is easily verified that such deformations are necessarily of the form

$$\mathbf{r}(u_1, u_2) = \mathbf{a}u_1u_2 + \mathbf{b}u_1 + \mathbf{c}u_2 + \mathbf{d}, \quad (11)$$

where $\mathbf{a} - \mathbf{d}$ are constant vectors.

The special case $\mathbf{a} = a\mathbf{e}_3$, $\mathbf{b} = b\mathbf{e}_1$, $\mathbf{c} = c\mathbf{e}_2$, $\mathbf{d} = \mathbf{0}$, where $\{\mathbf{e}_i\}$ is an orthonormal set, yields the classical hyperbolic paraboloid described by $r_3 = (a/bc)r_1r_2$. Accordingly, we refer to surfaces of the form (11) as generalized hyperbolic paraboloids, or, more succinctly, as *Hypar nets*.

3. A second-gradient model

The foregoing model suppresses the flexural and torsional resistance of the constituent fibers. The latter have recently been incorporated in [12, 13], using strain-energy functions of the form

$$W = w(\epsilon_L, \epsilon_M) + \frac{1}{2}A_L |L_\alpha L_\beta \mathbf{r}_{,\alpha\beta}|^2 + \frac{1}{2}A_M |M_\alpha M_\beta \mathbf{r}_{,\alpha\beta}|^2 + \frac{1}{2}A_\Gamma |L_\alpha M_\beta \mathbf{r}_{,\alpha\beta}|^2, \quad (12)$$

where $\mathbf{r}_{,\alpha\beta} = \partial^2 \mathbf{r} / \partial u_\alpha \partial u_\beta$ and A_L, A_M, A_Γ are positive material coefficients. Here $w(\epsilon_L, \epsilon_M)$ is the strain-energy function of conventional network theory. This form may be justified on the grounds that the second-order gradients $\mathbf{r}_{,\alpha\beta}$, when non-dimensionalized by a local length scale such as the spacing between adjacent fibers, the fiber diameters or the thickness of the sheet, are invariably small in typical applications. The leading-order contribution to the energy is then quadratic, provided that the network is relaxed in its undeformed state. The coefficients A_L , *etc.*, may conceivably depend on strains $E_{\alpha\beta}$. However, in the present work we confine attention to small strains. In this case the leading-order approximations to the coefficients A_L, A_M, A_Γ are (positive) constants. In these circumstances the strain-energy function (12) admits the Hypar network (11) as an equilibrium deformation field in the second-gradient theory. This is demonstrated below.

The modified energy involves three additional contributions, the physical significance of which is discussed in detail in [13]. In particular, the first and second contributions account for the normal and geodesic curvatures of the fibers and for the gradients of stretch along the fiber directions. Here we assume, for the sake of illustration, that these effects are controlled by two moduli, one for each fiber family. In general, for a given fiber family it is possible to attach separate moduli to each effect without affecting the basic structure of the theory. The third term of the modification accounts for twist of the fibers as the surface deforms, and for the cross derivatives of the fiber stretches in directions orthogonal to the fibers. The physical role of a cross derivative may be understood [33] in terms of the stretch it induces in an adjacent fiber that is parallel to the given fiber; eq. (12) attributes elastic energy to this effect. Moreover, inclusion of all three additional terms in the modified energy is sufficient to guarantee the convexity of the energy as a function of the $\mathbf{r}_{,\alpha\beta}$. This, in turn, is important for the well-posedness of the associated equilibrium problem.

In the absence of distributed loads the relevant equilibrium equation is again given by (6), but with \mathbf{T}_α replaced by [12]

$$\mathbf{T}_\alpha = \mathbf{N}_\alpha - \mathbf{M}_{\alpha\beta,\beta}, \quad (13)$$

where

$$\mathbf{N}_\alpha = \partial W / \partial \mathbf{r}_{,\alpha} \quad \text{and} \quad \mathbf{M}_{\alpha\beta} = \partial W / \partial \mathbf{r}_{,\alpha\beta}, \quad (14)$$

in which we note the symmetry $\mathbf{M}_{\alpha\beta} = \mathbf{M}_{\beta\alpha}$, inherited from that of $\mathbf{r}_{,\alpha\beta}$.

Edge conditions are naturally somewhat more complicated than their counterparts in the conventional theory. Specifically [12],

$$\mathbf{t} = \mathbf{T}_\alpha \nu_\alpha - (\mathbf{M}_{\alpha\beta} \nu_\alpha \tau_\beta)', \quad \boldsymbol{\mu} = \mathbf{M}_{\alpha\beta} \nu_\alpha \nu_\beta \quad \text{and} \quad \mathbf{f}_i = -[\mathbf{M}_{\alpha\beta} \nu_\alpha \tau_\beta]_i \quad (15)$$

are the edge traction, edge double force and point force at the i^{th} corner, respectively, the latter being operative at the corners of a piecewise smooth boundary. Here $(\cdot)' = d(\cdot)/ds$, where s measures counter-clockwise arclength on the boundary, $\tau_1 = -\nu_2$ and $\tau_2 = \nu_1$ are the components of the unit tangent to the edge, and the notation $[\cdot]$ stands for the jump as a corner is traversed; that is, $[\cdot] = (\cdot)_+ - (\cdot)_-$, where the subscripts “ \pm ” are used to denote limits as a corner located at arclength station s is approached through larger and smaller values of arclength, respectively.

The double force, which of course is absent in the elementary theory, generates the edge couple $\mathbf{c} = \mathbf{r}_\nu \times \boldsymbol{\mu}$, where $\mathbf{r}_\nu = \mathbf{r}_{,\alpha} \nu_\alpha$ is the normal derivative of the deformation at the edge. The double force should be understood as a distinct entity, however. In particular, it is not equivalent to the edge couple because the latter is sensitive only the part of the double force that is orthogonal to \mathbf{r}_ν .

Because $\mathbf{r}_{,\alpha}$ and $\mathbf{r}_{,\alpha\beta}$ are decoupled in the expression (12) for W , it follows that the \mathbf{N}_α coincide with the stress vectors (7) of the conventional theory. Accordingly, as shown in Section 2, the divergence $\mathbf{N}_{\alpha,\alpha}$ vanishes identically if the deformed surface is a Hypar net. Further, (12) and (14) imply that

$$\mathbf{M}_{\alpha\beta} = A_L L_\alpha L_\beta (L_\lambda L_\mu \mathbf{r}_{,\lambda\mu}) + A_M M_\alpha M_\beta (M_\lambda M_\mu \mathbf{r}_{,\lambda\mu}) + \frac{1}{2} A_\Gamma (L_\alpha M_\beta + M_\alpha L_\beta) (L_\lambda M_\mu \mathbf{r}_{,\lambda\mu}). \quad (16)$$

With $L_\alpha = \delta_{\alpha 1}$ and $M_\alpha = \delta_{\alpha 2}$, we may evaluate this for the deformation (11) to obtain

$$\mathbf{M}_{\alpha\beta} = \frac{1}{2}A_\Gamma(\delta_{\alpha 1}\delta_{\beta 2} + \delta_{\alpha 2}\delta_{\beta 1})\mathbf{a}. \quad (17)$$

Because these are constants, $\mathbf{M}_{\alpha\beta,\beta}$ vanishes and the equilibrium equation (6), with (13), is again satisfied. Thus Hypar nets also furnish equilibria in the present model.

Suppose, for example, that the initial plane is a rectangle with edges lying parallel to the fibers. On the right edge we have $\nu_\alpha = \delta_{\alpha 1}$ and hence the double force $\boldsymbol{\mu} = \mathbf{0}$; the edge couple therefore vanishes. The same is true on the top edge, where $\nu_\alpha = \delta_{\alpha 2}$, and also on the remaining two edges. The combination $\mathbf{M}_{\alpha\beta}\nu_\alpha\tau_\beta$ is easily seen to be constant on all four edges. Because $\mathbf{M}_{\alpha\beta,\beta}$ vanishes, the edge traction is then precisely the same as that required to support the Hypar net in the conventional theory. At the upper right and lower left corners, we compute the point force $\mathbf{f} = A_\Gamma\mathbf{a}$ using (15) and (17); the point force at the upper left and lower right corners is $\mathbf{f} = -A_\Gamma\mathbf{a}$. It follows that the Hypar net furnishes an equilibrium deformation in both the conventional and refined theories, and under the same boundary data, apart from the point forces required by the refined theory. These may be regarded as applied forces or as reactions provided by poles used to support the Hypar net.

In view of this finding, we devote the remainder of this work to a numerical study of the effects predicted by the refined theory when the boundary conditions are perturbed. For this purpose we assume the first term in (12) to be

$$w(\epsilon_L, \epsilon_M) = \frac{1}{2}(E_L\epsilon_L^2 + E_M\epsilon_M^2), \quad (18)$$

in accordance with the small-strain hypothesis, where $E_{L,M}$ are positive constants.

Because the refined theory represents a singular perturbation of the standard theory, we expect the effects of a perturbation of the boundary data to be localized near the edges of the network. This expectation is borne out in the examples.

4. Numerical simulations

In this section we discuss examples that are intended to highlight the differences between predictions based on the elementary and refined network theories. For this purpose we map the boundary of the undeformed network to a curve in three-dimensional space in accordance with (11). As we have shown, the deformation in the interior is also given by (11) in both theories, provided, in the case of a rectangular initial domain, that no double forces are applied in the refined theory and that suitable corner forces are present (see fig. (1)).

Using (18), the elementary theory predicts that the fibers of the network are in tension provided that the fiber stretches are both greater than unity. This is assured here, for a given reference configuration, by adjusting the vectors $\mathbf{a}, \mathbf{b}, \mathbf{c}$ in (11) accordingly. If a fiber stretch is less than unity at a given material point, then the fiber is under compression there and the entire deformation is unstable according to the energy criterion of elastic stability. This is proved in [5]. In this case the strain-energy function of the standard theory may be replaced by a suitable convexified function, constructed to ensure that the fibers are never in compression regardless of the values of the fiber stretches. This adjustment may be understood in terms of fine-scale wrinkling of the network [5, 34–36]. However, in the refined theory fiber compression would signal the onset of buckling. Fine-scale wrinkling is precluded in the refined theory due to the presence of an intrinsic length scale in the 2nd-gradient moduli A_L , *etc.*, which sets a length scale for the wavelength of a buckling pattern. The absence of an intrinsic length scale in the elementary theory implies the absence of a lower bound to the wavelength of a buckling pattern. This yields the prediction of a continuous distribution of wrinkles of infinitesimal amplitude in the (convexified)

elementary theory [5, 34]. The present 2nd-gradient model has been used in [37] to simulate buckling for various network geometries and to resolve the wavelengths of the associated buckling patterns.

The predicted deformations are obtained using the commercial software COMSOL MultiphysicsTM. This code furnishes a particularly convenient platform for our purpose, as it requires as input only the explicit expression for the strain-energy function. The program then constructs an associated weak form of the relevant equilibrium equations together with its finite-element implementation.

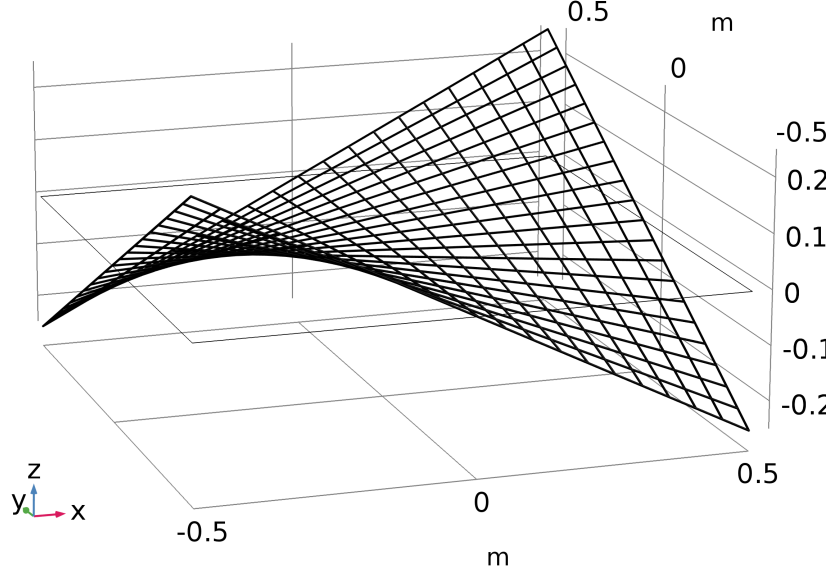


Figure 1. Square domain deformed by (11).

To simplify the analysis, a non-dimensional form of the problem is obtained by normalizing the strain energy with respect to a reference stiffness E_0 . All lengths are normalized with respect to a characteristic sample size L_0 . Using tildes to denote dimensionless quantities, the normalized constitutive parameters are:

$$\begin{aligned}\tilde{E}_L &= E_L/E_0, & \tilde{E}_M &= E_M/E_0, \\ \tilde{A}_L &= A_L/(E_0 L_0^2), & \tilde{A}_M &= A_M/(E_0 L_0^2), & \tilde{A}_\Gamma &= A_\Gamma/(E_0 L_0^2).\end{aligned}$$

In what follows, the dimensionless stiffnesses \tilde{E}_L and \tilde{E}_M are set to 100, and the values of the other stiffnesses are assumed to be equal. The latter values are specified in the captions to the figures.

We use a triangular mesh with interpolation functions of Argyris type. This kind of finite element is particularly well suited to energies that involve second gradient terms (see [13] for more details).

To illustrate the behavior of the network, we consider four shapes of the initial domain. Specifically, we study two square samples of unitary side, one cut along fiber directions and the other cut along the bias direction. We also study circular disc and a rectangular sample cut along the bias direction. In all the examples the fiber directions are assumed to coincide with the coordinate axes. Figure 2 displays the deformed equilibrium surfaces when boundary position is imposed in accordance with the restriction of (11) to the boundary and no double forces are applied.

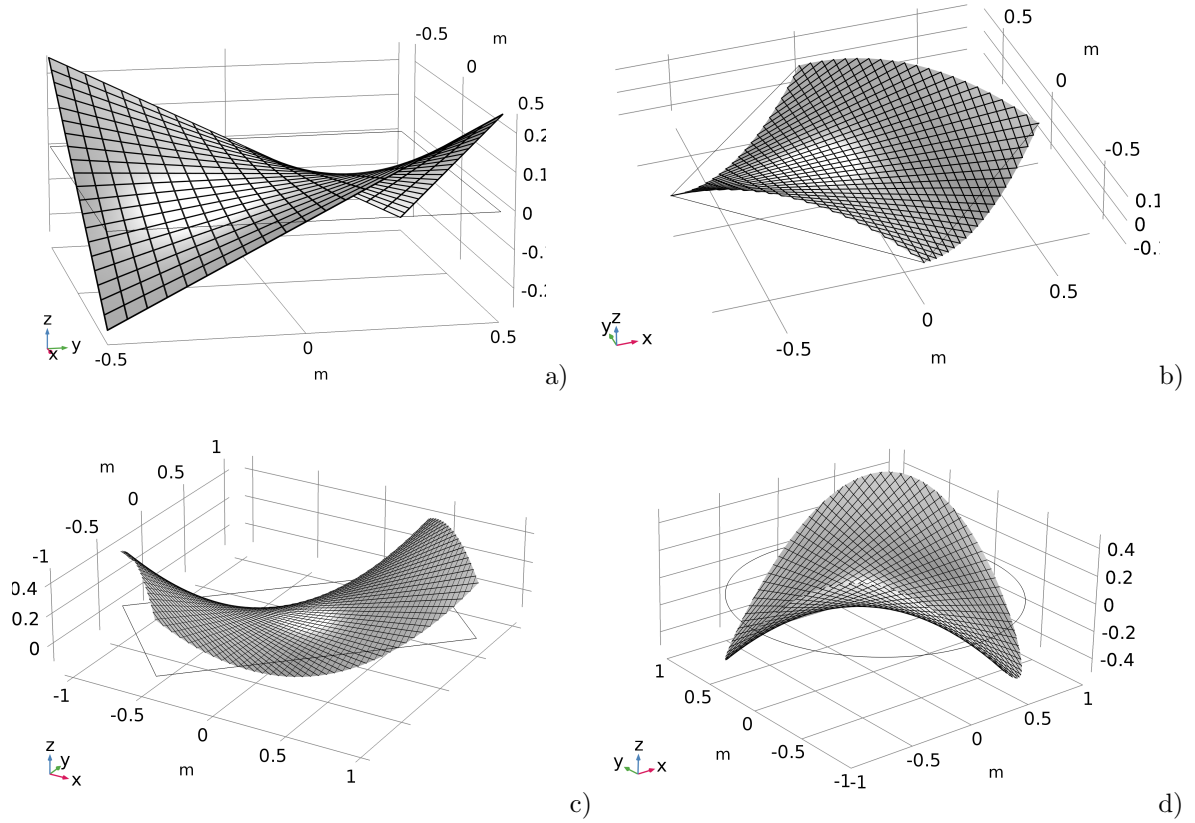


Figure 2. Plot deformed surfaces for various examples: a) square sample cut along fiber directions; b) square sample cut along the bias direction; c) rectangular sample cut along the bias direction; d) circular sample. Black solid lines represent current configurations of material lines.

Figures 3, 4 and 5, respectively, depict the deformations of the square and the rectangular samples cut along the bias direction as well as that of the circular disc. The plots exhibit the difference between the strain energies with and without the higher gradient terms for various values of the 2nd-gradient moduli and for the case of vanishing double force on the boundary. In each case the boundary is mapped, as before, in accordance with (11). In these examples the deformation (11) furnishes double forces on the boundary. For example, the double force is easily computed to be $\frac{1}{2} A_{\Gamma} \mathbf{a}$ on the upper right inclined edges of the square and rectangular samples. Relaxation of the double force on the boundary thus produces a deviation of the deformation relative to (11) in the interior of the network.

In the further examples, we assign the normal derivatives of the deformation at the boundaries. We consider the two cases: 1) the normal derivatives are zero, and 2) the normal derivatives are set to those induced by (11), multiplied by 0.5. Figures 6, 7, 8 and 9 depict the difference between the strain energy distributions with and without higher-gradient terms. In these numerical simulations, we assume $\hat{A}_L = \hat{A}_M = \hat{A}_{\Gamma} = 10$. Boundary effects associated with higher-gradient terms are seen to be localized near the corners of the square and rectangular samples, whereas for the circular disc these are widespread near the boundary.

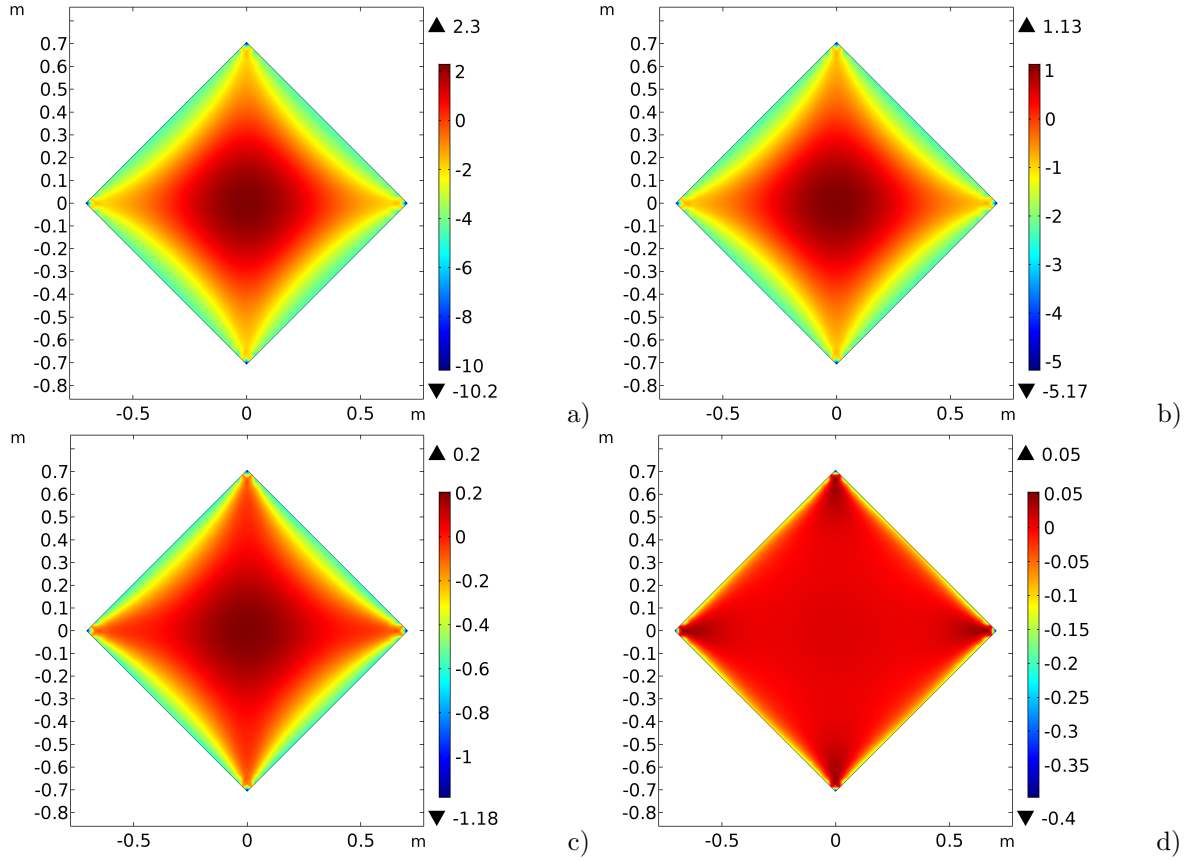


Figure 3. Plot of difference between strain energies with and without higher gradient terms: a) $\tilde{A}_L = \tilde{A}_M = \tilde{A}_\Gamma = 10$; b) $\tilde{A}_L = \tilde{A}_M = \tilde{A}_\Gamma = 5$; c) $\tilde{A}_L = \tilde{A}_M = \tilde{A}_\Gamma = 1$; d) $\tilde{A}_L = \tilde{A}_M = \tilde{A}_\Gamma = 0.1$.

5. Conclusion

The present model provides a simple and easily implemented refinement of the classical membrane theory of structural networks that accounts for the bending and twisting resistance of the fibers constituting a network. This affords a tool that may be used to assess the effects of variations in boundary conditions relative to those associated with the classical theory. Such variations may be interpreted as boundary imperfections that are inevitable in the actual realization of any network structure.

Acknowledgements

DJS gratefully acknowledges the support of the US National Science Foundation through grant CMMI 1538228.

References

- [1] W. Flügge. *Stresses in shells*, volume 2nd edn. Springer, Berlin, 1973.

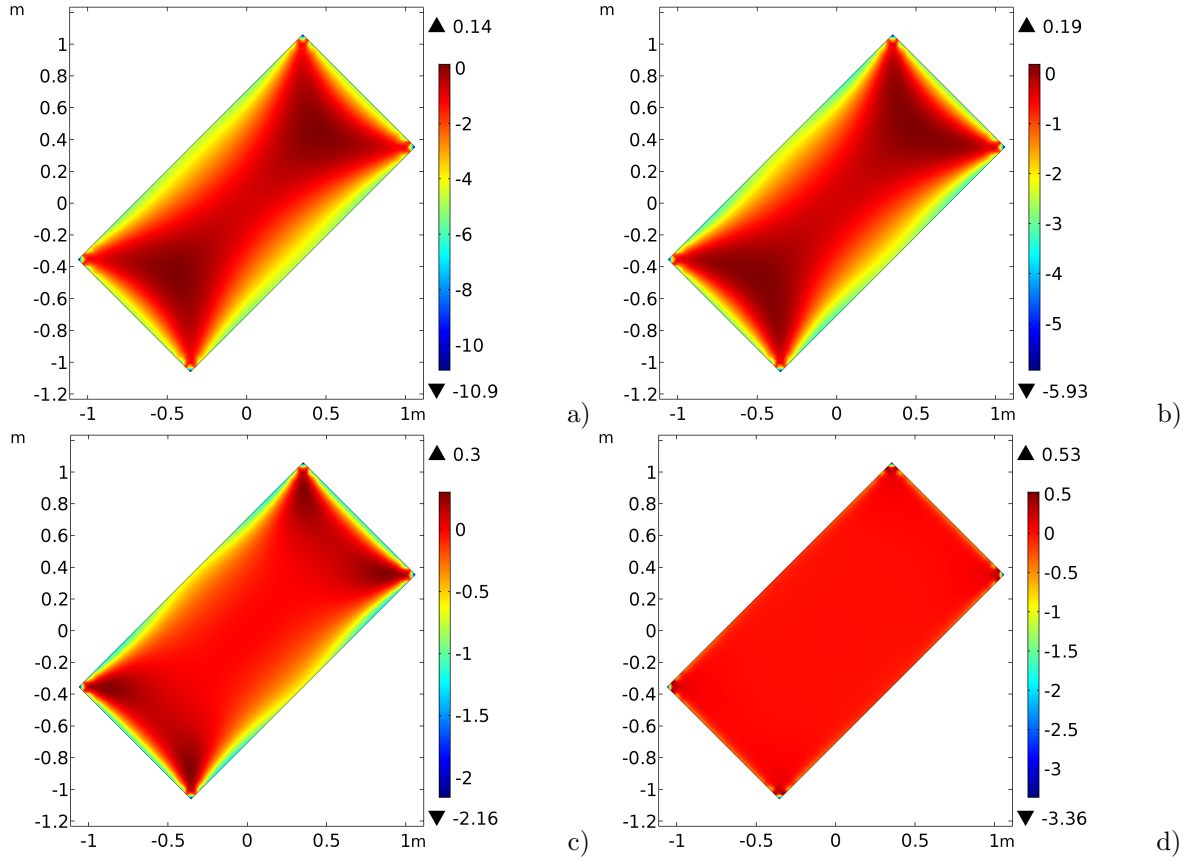


Figure 4. Plot of difference between strain energies with and without higher gradient terms: a) $\tilde{A}_L = \tilde{A}_M = \tilde{A}_\Gamma = 10$; b) $\tilde{A}_L = \tilde{A}_M = \tilde{A}_\Gamma = 5$; c) $\tilde{A}_L = \tilde{A}_M = \tilde{A}_\Gamma = 1$; d) $\tilde{A}_L = \tilde{A}_M = \tilde{A}_\Gamma = 0.1$.

- [2] F. Otto. Basic concepts and survey of tensile structures. *Tensile structures*, 2:11–96, 1966.
- [3] A. Viskovic. Hemp cables, a sustainable alternative to harmonic steel for cable nets. *Resources*, 7(4):70, 2018.
- [4] E. N. Kuznetsov. *Underconstrained structural systems*. Springer, NY., 2012.
- [5] D. J. Steigmann and A. C. Pipkin. Equilibrium of elastic nets. *Philosophical Transactions: Physical Sciences and Engineering*, pages 419–454, 1991.
- [6] P. Germain. The method of virtual power in continuum mechanics. Part 2: Microstructure. *SIAM Journal on Applied Mathematics*, 25(3):556–575, 1973.
- [7] R. D. Mindlin. Second gradient of strain and surface-tension in linear elasticity. *International Journal of Solids and Structures*, 1(4):417–438, 1965.
- [8] R. A. Toupin. Elastic materials with couple-stresses. *Archive for Rational Mechanics and Analysis*, 11(1):385–414, 1962.
- [9] F. dell’Isola, A. Della Corte, and I. Giorgio. Higher-gradient continua: The legacy of Piola, Mindlin, Sedov and Toupin and some future research perspectives. *Mathematics and Mechanics of Solids*, 22(4):852–872, 2017.
- [10] F. dell’Isola and P. Seppecher. Edge contact forces and quasi-balanced power. *Meccanica*, 32(1):33–52, 1997.
- [11] V. A. Eremeyev, F. dell’Isola, C. Boutin, and D. Steigmann. Linear pantographic sheets: Existence and uniqueness of weak solutions. *Journal of Elasticity*, 132(2):175–196, 2018.

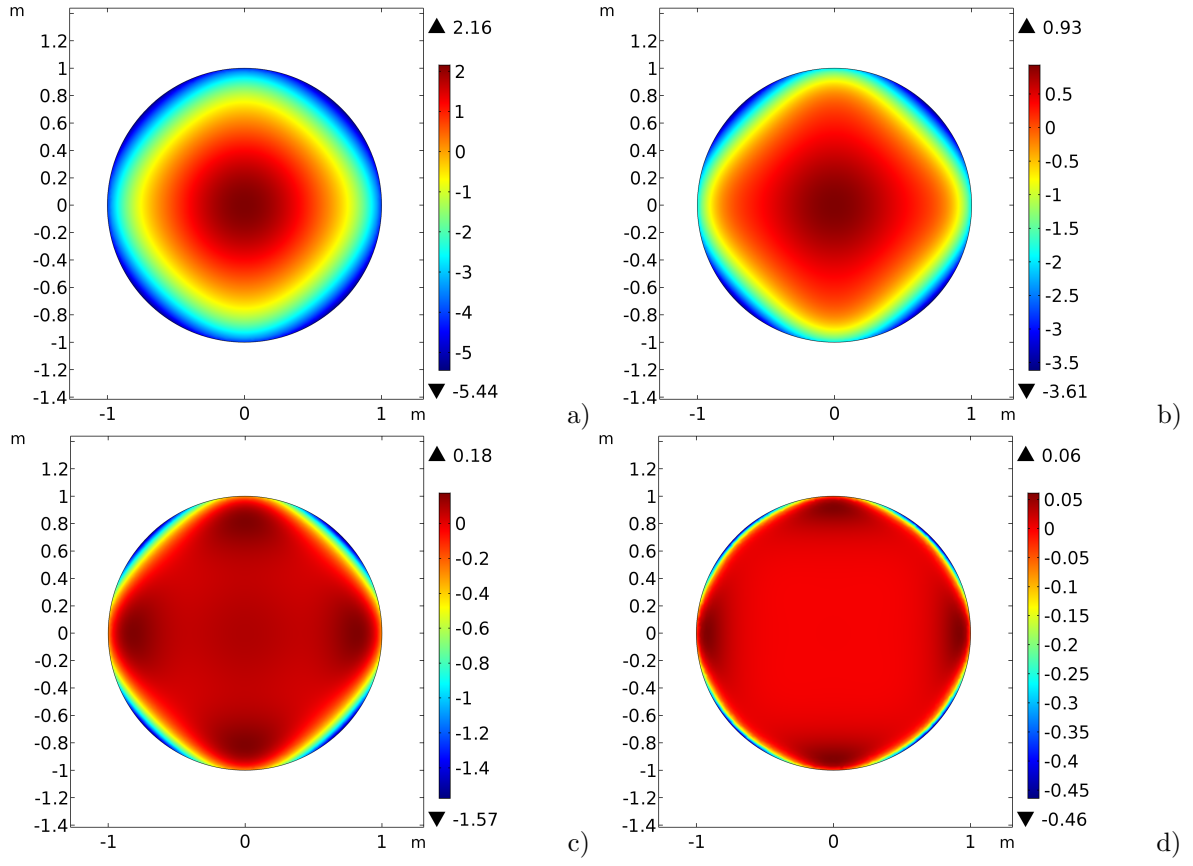


Figure 5. Plot of difference between strain energies with and without higher gradient terms: a) $\tilde{A}_L = \tilde{A}_M = \tilde{A}_\Gamma = 10$; b) $\tilde{A}_L = \tilde{A}_M = \tilde{A}_\Gamma = 5$; c) $\tilde{A}_L = \tilde{A}_M = \tilde{A}_\Gamma = 1$; d) $\tilde{A}_L = \tilde{A}_M = \tilde{A}_\Gamma = 0.1$.

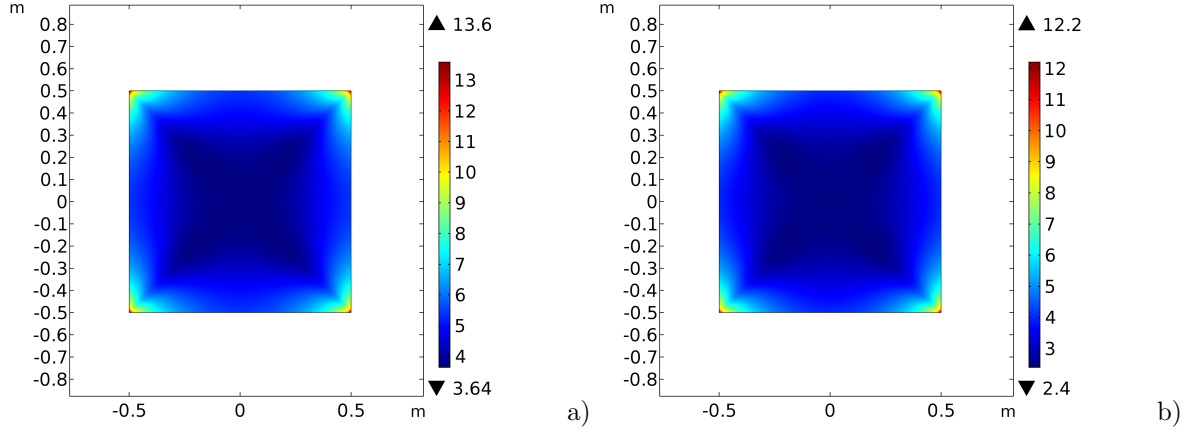


Figure 6. Plot of difference between strain energies with and without higher gradient terms, in the case of various normal derivative conditions at the boundary: a) zero normal derivatives; b) Hypar normal derivatives scaled by 0.5. Colors are in logarithmic scale.

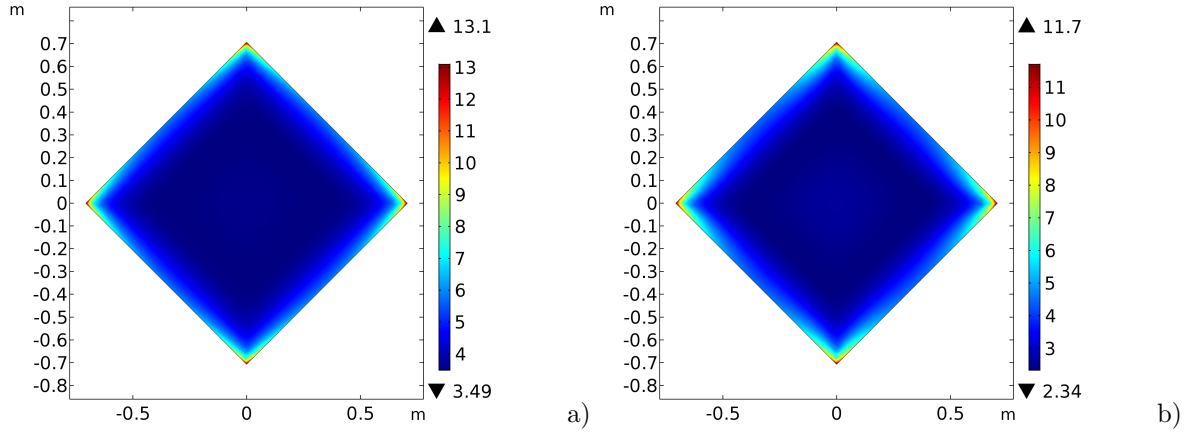


Figure 7. Plot of difference between strain energies with and without higher gradient terms, in the case of various normal derivative conditions at the boundary: a) zero normal derivatives; b) Hypar normal derivatives scaled by 0.5. Colors are in logarithmic scale.

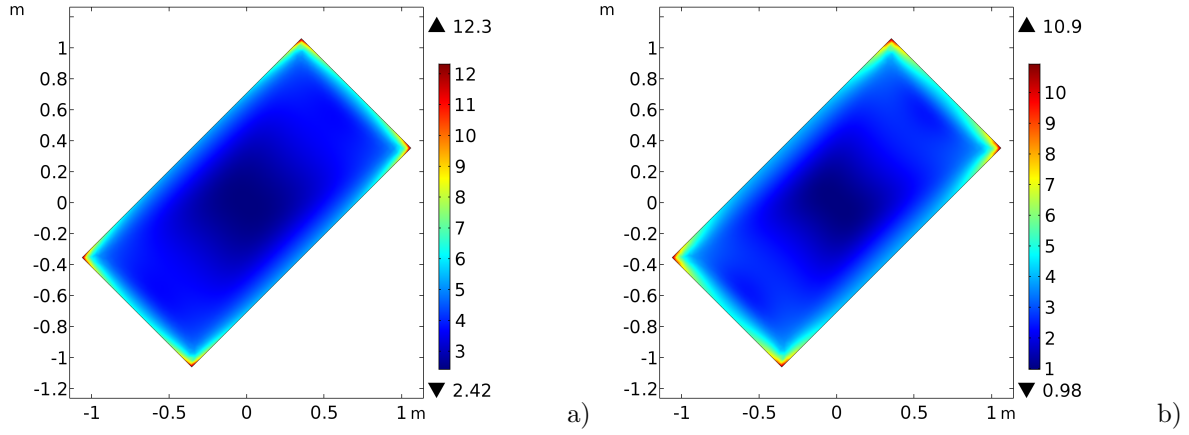


Figure 8. Plot of difference between strain energies with and without higher gradient terms, in the case of various normal derivative conditions at the boundary: a) zero normal derivatives; b) Hypar normal derivatives scaled by 0.5. Colors are in logarithmic scale.

- [12] D. J. Steigmann and F. dell'Isola. Mechanical response of fabric sheets to three-dimensional bending, twisting, and stretching. *Acta Mechanica Sinica*, 31(3):373–382, 2015.
- [13] I. Giorgio, R. Grygoruk, F. dell'Isola, and D. J. Steigmann. Pattern formation in the three-dimensional deformations of fibered sheets. *Mechanics Research Communications*, 69:164–171, 2015.
- [14] H. Abdoul-Anziz and P. Seppecher. Strain gradient and generalized continua obtained by homogenizing frame lattices. *Mathematics and mechanics of complex systems*, 6(3):213–250, 2018.
- [15] C. Pideri and P. Seppecher. A second gradient material resulting from the homogenization of an heterogeneous linear elastic medium. *Continuum Mechanics and Thermodynamics*, 9(5):241–257, 1997.
- [16] H. Abdoul-Anziz and P. Seppecher. Homogenization of periodic graph-based elastic structures. *Journal de l'École polytechnique – Mathématiques*, 5:259–288, 2018.
- [17] Y. Rahali, F. Dos Reis, and J.-F. Ganghoffer. Multiscale homogenization schemes for the construction of second-order grade anisotropic continuum media of architected materials. *International Journal for Multiscale Computational Engineering*, 15(1), 2017.

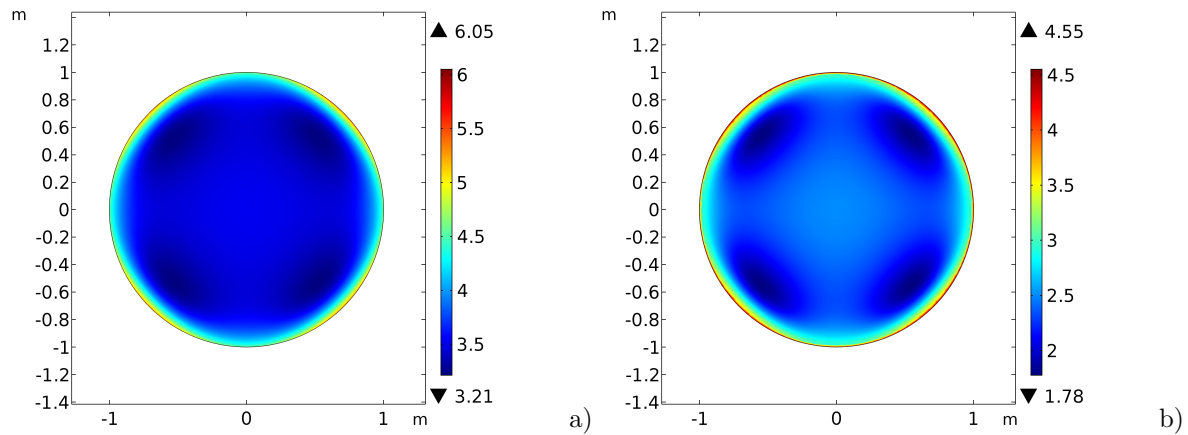


Figure 9. Plot of difference between strain energies with and without higher gradient terms, in the case of various normal derivative conditions at the boundary: a) zero normal derivatives; b) Hypar normal derivatives scaled by 0.5. Colors are in logarithmic scale.

- [18] Y. Rahali, J.-F. Ganghoffer, F. Chaouachi, and A. Zghal. Strain gradient continuum models for linear pantographic structures: a classification based on material symmetries. *Journal of Geometry and Symmetry in Physics*, 40:35–52, 2015.
- [19] J.-F. Ganghoffer, G. Maurice, and Y. Rahali. Determination of closed form expressions of the second-gradient elastic moduli of multi-layer composites using the periodic unfolding method. *Mathematics and Mechanics of Solids*, <https://doi.org/10.1177/1081286518798873>, 2018.
- [20] K. ElNady, I. Goda, and J.-F. Ganghoffer. Computation of the effective nonlinear mechanical response of lattice materials considering geometrical nonlinearities. *Computational Mechanics*, 58(6):957–979, 2016.
- [21] G. Rosi, L. Placidi, and N. Auffray. On the validity range of strain-gradient elasticity: a mixed static-dynamic identification procedure. *European Journal of Mechanics-A/Solids*, 69:179–191, 2018.
- [22] L. Placidi, E. Barchiesi, and A. Battista. An inverse method to get further analytical solutions for a class of metamaterials aimed to validate numerical integrations. In *Mathematical Modelling in Solid Mechanics*, pages 193–210. Springer, 2017.
- [23] A. Misra and P. Poorsolhjouy. Identification of higher-order elastic constants for grain assemblies based upon granular micromechanics. *Mathematics and Mechanics of Complex Systems*, 3(3):285–308, 2015.
- [24] E. Turco, A. Misra, R. Sarikaya, and T. Lekszycki. Quantitative analysis of deformation mechanisms in pantographic substructures: experiments and modeling. *Continuum Mechanics and Thermodynamics*, <https://doi.org/10.1007/s00161-018-0678-y>:1–15, 2018.
- [25] E. Turco, M. Golaszewski, A. Cazzani, and N. L. Rizzi. Large deformations induced in planar pantographic sheets by loads applied on fibers: experimental validation of a discrete lagrangian model. *Mechanics Research Communications*, 76:51–56, 2016.
- [26] L. Greco and M. Cuomo. On the force density method for slack cable nets. *International Journal of Solids and Structures*, 49(13):1526–1540, 2012.
- [27] L. Greco, N. Impollonia, and M. Cuomo. A procedure for the static analysis of cable structures following elastic catenary theory. *International Journal of Solids and Structures*, 51(7-8):1521–1533, 2014.
- [28] J. Altenbach, H. Altenbach, and V. A. Eremeyev. On generalized Cosserat-type theories of plates and shells: a short review and bibliography. *Archive of Applied Mechanics*, 80(1):73–92, 2010.
- [29] L. Placidi, E. Barchiesi, E. Turco, and N. L. Rizzi. A review on 2D models for the description of pantographic fabrics. *Zeitschrift für angewandte Mathematik und Physik*, 67(5):121, 2016.
- [30] F. dell’Isola et al. Pantographic metamaterials: an example of mathematically driven design and of its technological challenges. *Continuum Mechanics and Thermodynamics*, <https://doi.org/10.1007/s00161-018-0689-8>, 2018.

- [31] L. Placidi, L. Greco, S. Bucci, E. Turco, and N. L. Rizzi. A second gradient formulation for a 2D fabric sheet with inextensible fibres. *Zeitschrift für angewandte Mathematik und Physik*, 67(5):114, 2016.
- [32] W. A. Green and J. Shi. Plane deformations of membranes formed with elastic cords. *The Quarterly Journal of Mechanics and Applied Mathematics*, 43(3):317–333, 1990.
- [33] F. dell’Isola and D. Steigmann. A two-dimensional gradient-elasticity theory for woven fabrics. *Journal of Elasticity*, 118(1):113–125, 2015.
- [34] E. M. Haseganu and D. J. Steigmann. Equilibrium analysis of finitely deformed elastic networks. *Computational mechanics*, 17(6):359–373, 1996.
- [35] I. Giorgio, P. Harrison, F. dell’Isola, J. Alsayednoor, and E. Turco. Wrinkling in engineering fabrics: a comparison between two different comprehensive modelling approaches. *Proceedings of the Royal Society A. Mathematical, physical, and engineering sciences*, 474(2216):20 pages, 2018.
- [36] E. Barchiesi, G. Ganzosch, C. Liebold, L. Placidi, R. Grygoruk, and W. H. Müller. Out-of-plane buckling of pantographic fabrics in displacement-controlled shear tests: experimental results and model validation. *Continuum Mechanics and Thermodynamics*, pages 1–13, 2018.
- [37] I. Giorgio, A. Della Corte, F. dell’Isola, and D. J. Steigmann. Buckling modes in pantographic lattices. *Comptes rendus Mecanique*, 344(7):487–501, 2016.